Atomistic insights into the lung cancer-associated L755P mutation in HER2 resistance to lapatinib: a molecular dynamics study

Bei Yang · Haiping Zhang · Hao Wang

Abstract HER2, a member of the human ErbB protein family belonging to receptor tyrosine kinases, plays important roles in regulating crucial cellular processes, including cell migration, proliferation, and differentiation. A missense mutation, L755P, in the HER2 kinase domain has been involved in lung cancer in humans and exhibits reduced response to lapatinib therapy. However, the detailed mechanism of how the HER2 L755P mutation causes drug resistance to lapatinib remains elusive. Here, molecular docking, molecular dynamics (MD) simulations, binding free energy calculations [molecular mechanics and generalized Born/surface area (MM-GBSA)] were performed to reveal the mechanism of drug resistance due to the HER2 L755P mutation. MD simulations revealed that the L755P mutation caused structural changes in the regions of helix αC, the glycine-rich loop, and the activation loop, thereby leading to the loss of interactions between the solubilizing group of lapatinib and HER2. Moreover, MM-GBSA calculations suggested that hydrophobic interactions between lapatinib and HER2 contribute most to the binding affinity, and that the L755P mutation could result in a less energetically favorable HER2/lapatinib complex. This may weaken the binding of lapatinib to the mutated HER2, thereby leading to the emergence of drug resistance. This study offers a structural explanation for the effect of the L755P mutation on the HER2/lapatinib complex.

Bei Yang and Haiping Zhang wish it to be known that, in their opinion, the first two authors should be regarded as joint first authors

B. Yang · H. Wang (✉)
Department of Thoracic Surgery, Shanghai Pulmonary Hospital, Tongji University, Shanghai 200433, China
e-mail: haowang_1980@163.com

H. Zhang
Department of Oncology, Shanghai Pulmonary Hospital, Tongji University, Shanghai 200433, China

Introduction

Receptor tyrosine kinases (PTKs) are cell surface receptors that play a pivotal role in intercellular communication and oncogenesis [1]. Currently, about 20 distinct classes of PTKs have been identified. The human ErbB protein family or epidermal growth factor receptor (EGFR) family—one class of PTKs—includes four members: EGFR (ErbB1), HER2 (ErbB2), HER3 (ErbB3), and HER4 (ErbB4) [2]. In this family, ligands such as growth factors binding to the extracellular ligand-binding domains promote receptor homo- or hetero-dimerization [3]. This process results in activation of the catalytic kinase domains, which in turn can interact with downstream proteins to regulate crucial cellular processes, encompassing cell migration, proliferation, and differentiation [4, 5]. Amplification or overexpression of the ErbB protein family has been frequently associated with a host of human diseases, including lung, breast, and gastric cancers [6]. Therefore, the ErbB protein family is gaining increasing interest as a therapeutic antitumour target both in academia and in drug development in the pharmaceuticals industry.

All members of the ErbB protein family are composed of similar overall structural domains, including an extracellular ligand binding domain, a signal transmembrane α-helix domain, an intracellular tyrosine kinase domain to which the ATP binds, and a C-terminal tail where phosphorylation occurs [7]. From a drug design standpoint, it is not unreasonable to sculpt small molecule ATP competitive inhibitors to exclude ATP

from the ATP-binding site of the tyrosine kinase domain, thereby eradicating phosphorylation and causing aberrant subsequent downstream signal transduction. These principles lay the foundation for the design and development of ErbB protein family inhibitors for cancer treatment. To date, several drugs based on ATP competitive inhibitors have appeared on the market that target the ErbB protein family. For example, erlotinib (Tarceva) and gefitinib (Iressa) function as ATP-competitive inhibitors of EGFR to treat non-small cell lung cancer [8]. Lapatinib (Tykerb) acts as a dual HER2/EGFR inhibitor that is used for breast cancer and several solid tumours [9].

It is well documented that the use of targeted therapies to specifically inhibit an oncogenic kinase can lead to selective pressure on the tumor to overcome the inhibition through the emergence of a drug-resistant mutation [6]. As in the case of Bcr-Abl oncogenic fusion protein, the gatekeeper mutation T344I in the tyrosine kinase domain renders the drug imatinib (Gleevec) ineffective against chronic myelogenous leukemia and subsequently leads to clinical relapse following treatment with imatinib [10]. In a similar vein, the gatekeeper mutation T790M, similar to the T344I mutation in Bcr-Abl kinase, has also been found in EGFR, causing drug resistance to erlotinib or gefitinib [11]. Apart from the gatekeeper mutation, several clinical drug-resistant mutations located in the ATP-binding site of EGFR tyrosine kinase domain have also been observed, e.g., C775F and T854A [12]. Numerous computational and experimental studies have been performed to gain mechanistic and structural insights into the origin of drug-resistant mutations in the EGFR, such as decreased affinity for the erlotinib or gefitinib and increased affinity for the binding of ATP to the EGFR T790M mutant [13], steric clashes due to the EGFR C775F mutation [12], and a loss of interaction as a result of the EGFR T854A mutation [14].

As with HER2, recent evidence has revealed that somatic mutations in the HER2 kinase domain are closely correlated to many solid tumor types, such as breast and lung [15, 16]. Stenphen et al. [17] found that an activating missense mutation, L755P, in the HER2 kinase domain has an inextricable link to lung cancers in humans. As a result, this mutation, which is located at the ATP-binding site, exhibited a reduced response to lapatinib therapy. However, the detailed mechanism of how the HER2 L755P mutation causes drug-resistance to lapatinib remains currently unknown. To investigate this mechanism, we carried out molecular docking, molecular dynamics (MD) simulations, and binding free energy calculations [molecular mechanics and generalized Born/surface area (MM-GBSA)] to uncover the molecular basis underlying

drug-resistance due to the HER2 L755P mutation. Understanding the origin of drug-resistance has benefits for designing the next generation of selective and potent HER2 inhibitors.

Methods

Model setup

The 2.2 Å crystal structure of human HER2 kinase domain in complex with its ATP competitive inhibitor SYR127063 was extracted from the RCSB Protein Data Bank (PDB ID: 3PP0) [18]. The absent residues (residues: Asp880–Gly881) in the activation loop (A loop) was modeled using the MODELLER program [19]. The construction of the HER2 L755P mutant was performed by the replacement of target residue L755 with the desired residue P755. The chemical structure for the lapatinib was built by the ACD/ChemSketch software and subsequently energy-minimized using the B3LYP/6-31G* as implemented in the program Gaussian03 [20].

Molecular docking

The inhibitor SYR127063 was ruled out from the HER2-SYR127063 complex and the resulting unbound structure was utilized in the docking study, which was conducted using the AutoDock4.2 package [21]. For the HER2 kinase, the polar hydrogen atoms were added and subsequently the Kollman united atom partial charges and AutoDock atom types were assigned. For the inhibitor lapatinib, all hydrogen atoms including polar and non-polar atoms were added and the Gasteiger-Hückel atomic charge was then assigned. The grid center was defined at the centroid of the SYR127063 in the HER2-SYR127063 complex. The number of grid points in the x, y, and z direction was set to 70, 70, and 70 with a spacing value of 0.375 Å. The Lamarckian genetic algorithm was used for ligand conformational search; the parameters were set the same in the previous studies reported by Lu et al. [22, 23]. Fifty independent docking experiments were performed and the binding energy was used to rank the docked ligand in order of fitness.

MD simulations

MD simulations of the two systems, HER2-lapatinib and L755P HER2-lapatinib complexes, were conducted using the AMBER11 package [24]. The AMBER ff03

force field [25] was used for the HER2 and the inhibitor lapatinib was described by the generalized AMBER force field (GAFF) [26]. The electrostatic potential for the lapatinib was calculated at the HF/6-31G* level using the program Gaussian03 [20]. Thereafter, the partial charges for the lapatinib were determined through the restricted electrostatic-potential fitting method (RESP) encoded in the Antechamber module of AMBER11. A truncated octahedral box of TIP3P waters [27] was added with a 10 Å buffer around the complex. Two Cl^- counter-ions were added to maintain the electroneutrality of the two simulated systems.

In the minimization of the systems, the HER2-lapatinib complex was first constrained to minimize the water molecules and counterions (the steepest descent for the first 2,500 steps and then the conjugated gradient for the next 2,500 steps). The whole system was then minimized without any restraint (the steepest descent for the first 5,000 steps and then the conjugated gradient for the next 5,000 steps). Thereafter, each system was heated to 300 K in 150 ps followed by constant temperature equilibration at 300 K for 300 ps. In the production process, each 100 ns MD simulation was performed in an isothermal isobaric ensemble (NPT) with periodic boundary conditions. An integration step of 2 fs was set and the particle mesh Ewald (PME) method [28], using a cubic fourth-order B-spline interpolation, was used to calculate the long-range electrostatic interactions. A cut-off distance of 10 Å was used to calculate the short-range electrostatics and van der Waals interactions. SHAKE [29] was used to restrain all covalent bonds involving hydrogen atoms. Each simulation was coupled to a 300 K thermal bath at 1.0 atm by means of the Langevin algorithm [30].

MM-GBSA calculations

MM-GBSA calculations were used in the last 50 ns trajectories of the two simulations [31–34]. The 101 snapshots were chosen from the 50–100 ns MD trajectory with an interval of 50 ps to calculate binding free energy ($\Delta G_{\text{binding}}$) between HER2 and lapatinib. $\Delta G_{\text{binding}}$ was calculated using Eq. (1).

$$DG_{\text{binding}} = DG_{\text{complex}} - \left[DG_{\text{protein}} + DG_{\text{ligand}} \right] \tag{1}$$

Each free energy term in Eq. (1) consists of the gas phase molecular mechanical energy (ΔE_{gas}), the solvation free energy ($\Delta G_{\text{solvation}}$) and the entropy term ($-T\Delta S$), using Eq. (2). The conformational entropy

($-T\Delta S$) was calculated through a normal mode analysis with AMBER NMODE module.

$$DG_{\text{binding}} = DE_{\text{gas}} + DG_{\text{solvation}} - TDS \tag{2}$$

ΔE_{gas} can be further divided into the van der Waals energy (ΔE_{vdW}), electrostatic energy (ΔE_{ele}), and internal energy (ΔE_{int}) in the gas phase [Eq. (3)].

$$DE_{\text{gas}} = DE_{\text{vdW}} + DE_{\text{ele}} + DE_{\text{int}} \tag{3}$$

The solvation free energy, $\Delta G_{\text{solvation}}$, consists of two parts [Eq. (4)]: the polar contribution (ΔG_{GB}) and the nonpolar contribution ($\Delta G_{\text{nonpolar}}$).

$$DG_{\text{solvation}} = DG_{\text{GB}} + DG_{\text{nonpolar}} \tag{4}$$

The polar contribution (ΔG_{GB}) to the solvation free energy was obtained using the GB model described by Onufriev et al. [51] (igb=5) with mbondi2 radii and interior and exterior dielectric constants of 1 and 78.5, respectively. The nonpolar contribution ($\Delta G_{\text{nonpolar}}$) to the solvation free energy was calculated from the solvent-accessible surface-area (SASA) [Eq. (5)],

$$\Delta G_{\text{nonpolar}} = g' \text{SASA} + b \tag{5}$$

The corresponding solvation parameters γ and b are 0.0072 kcal mol^{-1} $Å^{-2}$ and 0 kcal mol^{-1}, respectively.

Residue-ligand pairs interaction decomposition

The binding energies were decomposed into contributions from HER2 and lapatinib interaction pairs, which can only use the MM-GBSA method. The binding energy of each interaction pair is composed of three terms: $\Delta E\text{vdW}$, ΔE_{ele} and ΔG_{GBSA}.

Cluster analysis

Cluster analysis of the MD trajectory was carried out to group together coordinate snapshots from the trajectory into distinct sets by virtue of the average-linkage algorithm reported by Shao et al. [35]. Pairwise C_α atoms root-mean-square deviation (RMSD) comparisons were performed between any snapshot and the average coordinate after rigid-body alignment using a threshold of 1.5 Å.

Cross-correlation analyses

The dynamic features of the protein in MD simulations can be analyzed to produce information that is pertinent to correlated motions, which can be described as a network of interacting residues and also between regions as in domain–domain communication. Generally, the cross correlation, described by the $C(i,j)$ [Eq. (6)], of C_α atoms was used to reveal correlative motions of proteins.

$$C(i,j) = \frac{c(i,j)}{c(i,i)^{1/2} c(j,j)^{1/2}} \qquad (6)$$

The obtained elements $C(i,j)$ can be exhibited as a three-dimensional (3D) dynamical cross-correlation map [36, 37].

Results

Similar to other protein kinases, the HER2 tyrosine kinase domain consists of a smaller N-terminal lobe (N-lobe) and a larger C-terminal lobe (C-lobe). As shown in Fig. 1a, the N-lobe is composed of five anti-parallel β-sheets and one helix, also named as helix αC. The conformational transition of helix αC plays an important role in the activation process of protein kinases [38, 39]. The C-lobe is composed mainly of α-helices. The ATP-binding site, which is highly conserved in the protein kinase family, is located between the N- and C-lobes underneath the glycine-rich nucleotide positioning motif, also called the G loop. It is well-known that in numerous serine/threonine/tyrosine protein kinases, phosphorylation of the activation loop (A loop) acts as a phosphorylation-

sensitive switch for access of ATP and substrate to the active site cleft, which allows proper alignment of the N- and C-terminal lobes for catalysis [40]. Conversely, in the unphosphorylated paradigm, ATP and substrate access to the catalytic groove are sterically hindered as a result of the disordered A loop folding into the active site cleft. In the ErbB protein family, however, phosphorylation of the A loop is not required for kinase activation. Rather, it is activated through an allosteric mechanism [18]. Therefore, in the HER2 unphosphorylated state, the A loop is still in the ordered, active kinase conformation and runs through the surface of the catalytic cleft. The residue L755, proximal to the ATP-binding site, is located in a loop connecting the β3 sheet to helix αC.

Molecular docking study

Recently, Aertgeerts et al. [18] solved the co-crystal structure of the HER2/SYR127063 complex, yet the co-crystal structure of the HER2/lapatinib complex remains unavailable. As shown in Fig. 1b, the chemical structures of SYR127063 and lapatinib are similar overall, indicating that the interactions of lapatinib with HER2 may resemble those of SYR127063 with HER2. Based on this hypothesis, we used molecular docking to model the interactions between lapatinib and HER2. Figure 1c shows the lowest binding energy between the docked lapatinib and HER2 derived from the largest cluster. Overall, the binding modes between lapatinib and HER2 are consistent with the co-crystal structure of the HER2/SYR127063 complex with the exception of the solubilizing group. In the HER2/SYR127063 complex (Fig. 1a), the solubilizing group of the SYR127063 is located under the G loop and is shielded from the solvent. In contrast, in the docked HER2/lapatinib complex (Fig. 1c), the solubilizing group of lapatinib protrudes into the
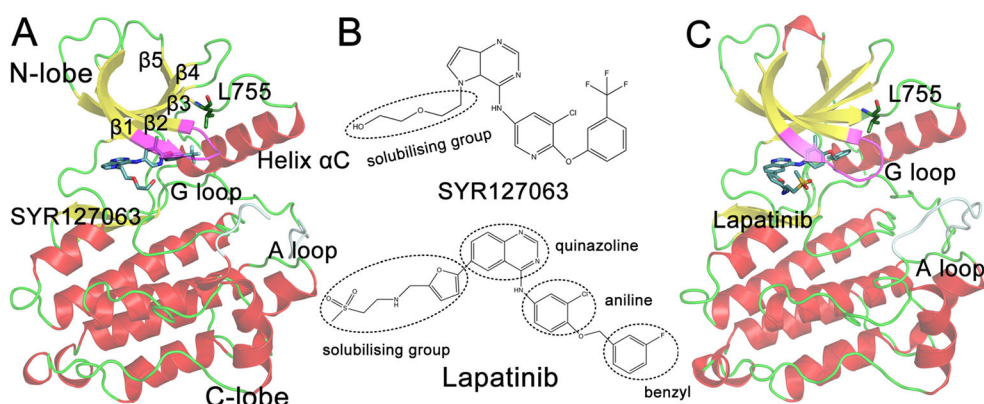

Fig. 1 **a** Cartoon representation of the secondary structure of the HER2/SYR127063 complex (PDB ID: 3PP0). Structures: *Yellow* loop, *green* β-sheet, *red* α-helix, *magenta* G loop, *light blue* A loop. SYR127063 in the ATP-binding site and residue L755 are shown by sticks. **b** Chemical structures of SYR127063 and lapatinib. **c** The docked structure of HER2/lapatinib complex with the lowest binding energy in the largest cluster. Lapatinib in the ATP-binding site and is shown by sticks. Colors as in **a**

solvent. We next performed MD simulations to explore the dynamic characteristics of lapatinib in the ATP-binding site and to investigate the mechanism of drug-resistance due to the L755P mutation.

System behavior and convergence

Conventional 100 ns MD simulations were conducted for the wild-type (WT) HER2/lapatinib and L755P HER2/lapatinib complexes in the explicit solvent, respectively. To reveal convergence of the simulated systems, the RMSD of the Cα atoms of the simulated protein in relation to the initial structure was monitored. As shown in Fig. 2a, fluctuation of the RMSD plot for the WT system was similar throughout the simulation, with the RMSD value of 2.3±0.2 Å. In the L755P system, in the first 30 ns of simulation, the behavior of the mutated protein was similar to that of the WT system, with the RMSD value of 2.2±0.2 Å. However, thereafter the mutated protein underwent a slightly larger fluctuation compared to the WT system. The RMSD value for the L755P system was calculated to be 2.9±0.2 Å in the range from 30 to 100 ns simulation. This suggests that the L755P mutation causes a conformational change in HER2. On the basis of the RMSD analysis, the first 30 ns MD trajectory was deleted and the remaining 70 ns trajectory was used in the production analysis.

To reveal the effect of the L755P mutation on specific domain dynamics, the root-mean-square fluctuation (RMSF) for the Cα atoms of the simulated protein was assessed. As shown in Fig. 2b, the A loop in both systems showed the largest fluctuation, revealing the conformational

plasticity of the A loop. This dynamic property is in good agreement with the crystal observation that the A loop structure changes from a disordered conformation to an ordered conformation during transition of the kinase from the inactive to the active state [41]. Overall, compared to the WT system, the regions of the A loop, G loop, and helix αC displayed significantly larger fluctuations in the mutated system. These data indicated that the L755P mutation caused conformational changes mainly in the above three regions, laying the foundation for the subsequent structural analysis.

Structural analysis

As seen above, significant differences in the dynamic behaviors of HER2 in the WT and mutated states exist in the A loop, G loop, and helix αC. Therefore, in the structural analysis, we focused primarily on these regions. The most representative structure obtained from the WT and L755P systems was obtained using cluster analysis of each MD trajectory. Figure 3 shows the backbone superimposition of the representative structures of the WT and L755P systems. Consistent with the RMSF analysis, the regions of the A loop, G loop, and helix αC showed notable changes, with only small differences in other domains. Due to the specific properties of Pro residues, the mutation of native residues to Pro residues would cause local structural changes in the proximity of the mutation site. As shown in Fig. 3, compared to the WT system, the N-terminus of the helix αC in the L755P mutated system experienced pronounced conformational change and moved toward the G loop, leading to the collapse of the G loop into

Fig. 2 **a** The root-mean-square deviation (RMSD) of Cα atoms of HER2 for the WT HER2/lapatinib complex (*black*) and L755P HER2/lapatinib complex (*red*) as a function of 100-ns molecular dynamics (MD) simulations. **b** The root-mean-square fluctuation (RMSF) of Cα atoms of HER2 for the WT HER2/lapatinib complex (*black*) and L755P HER2/lapatinib complex (*red*)
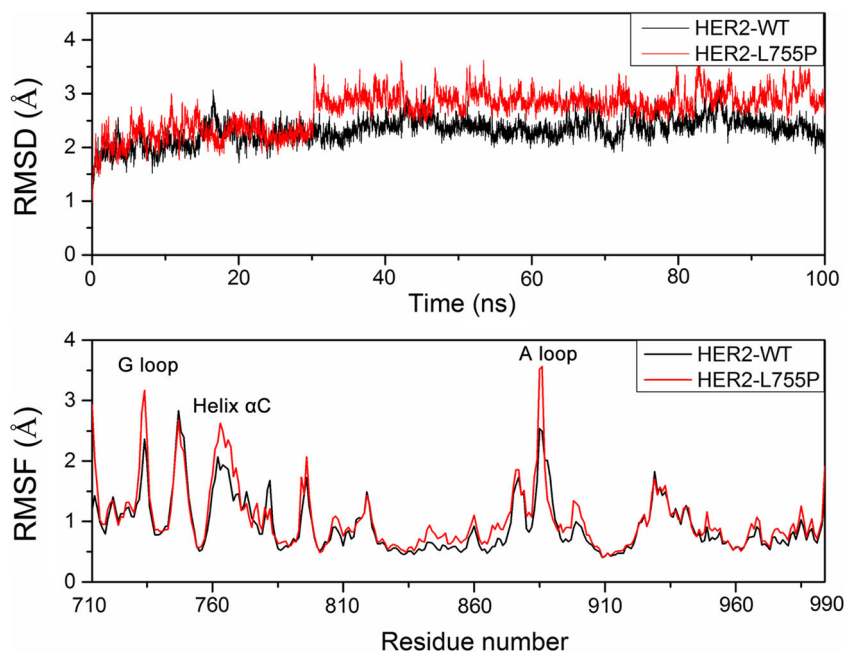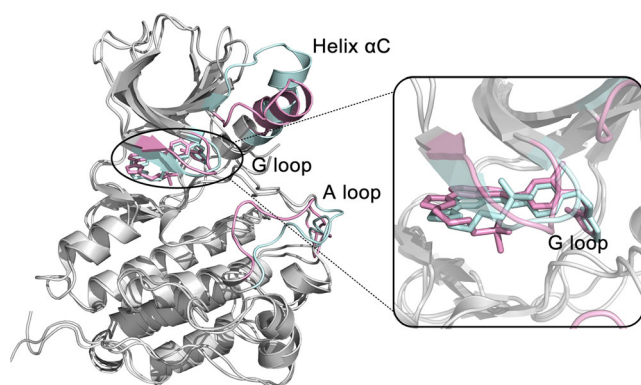
Fig. 3 a The backbone superimposition of the representative structure obtained from MD simulations between the WT and L755P systems. The conformations of the helix αC, G loop, and A loop in the WT and L755P systems are colored in *light cyan* and *pink*, respectively. The *expanded region* shows the orientation of lapatinib in the ATP-binding site in the WT and L755P systems. Lapatinib in the WT and L755P systems is colored in *light cyan* and *pink*, respectively

the ATP-binding site. In addition, the backbone structures of the crystal structure of the HER2/SYR127063 complex was superimposed with that of the MD snapshot of the HER2/lapatinib complex to reveal the dynamic behavior of lapatinib. As shown in Fig. 4, in both systems the solubilizing group of lapatinib was located in the ATP-binding site below the G loop and shielded from the solvent, which is in agreement with the position of the solubilizing group of SYR127063 in the co-crystal structure of the HER2/SYR127063 complex [18]. Upon close examination of the detailed interactions between lapatinib and HER2 in
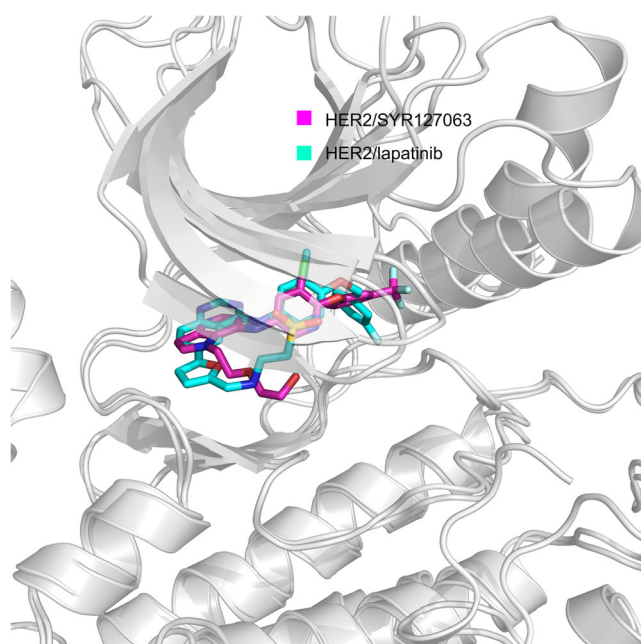
the two simulated systems, we found that, in the WT system, the solubilizing group of lapatinib pointed toward to the G loop and formed close contacts with residues in the G loop. Conversely, in the L755P mutated system, the solubilizing group of lapatinib oriented towards the interior of the ATP-binding site and formed no contacts with the G loop. The remarkable difference in the orientation of the solubilizing group of lapatinib in the two systems may be ascribed to the distinct dynamic behavior of the G loop, whereas in the L755P mutated system the G loop collapsed into the ATP-binding site. The interactions of the remaining moieties of lapatinib with HER2 showed no significant differences between the two systems. Therefore, disruption of the interactions between the solubilizing group of lapatinib and HER2 induced by the L755P mutation may lead to drug resistance to lapatinib, which can be tested by the following binding free energy analysis.

Binding free energy calculations

The binding free energies ($\Delta G_{binding}$) between lapatinib and HER2 in the WT and L755P systems were calculated by the MM-GBSA method, which has been used widely to elucidate variation in binding affinities between proteins and ligands/proteins in biomolecules [31–34]. Table 1 lists the free energy components for $\Delta G_{binding}$. The favorable energy contributions to the binding of lapatinib to HER2 were derived from the van der Waals (ΔE_{vdW}) and the electrostatic (ΔE_{ele}) items of the molecular mechanics energy, coupled with the nonpolar item

Fig. 4 The backbone superimposition of HER2/SYR127063 (*magenta*) and HER2/lapatinib (*cyan*) (100 ns snapshot from MD simulation)

Table 1 Binding free energy analysis (kcal mol) for the interactions between Lapatinib and the wild-type HER2 and L755P mutant[a]

Energy items	Complexes		
	WT	L755P mutant	*P*-value[e]
ΔE_{ele}	−28.48(4.44)	−22.64(4.64)	1.37E-16
ΔE_{vdW}	−67.15(3.04)	−62.78(3.52)	1.93E-17
$\Delta G_{nonpolar}$	−8.07(0.22)	−8.96(0.25)	2.90E-67
ΔG_{polar}	48.44(3.37)	46.80(3.96)	1.96E-03
ΔG_{sol}[b]	40.37(3.27)	37.84(3.83)	1.27E-06
ΔG_{ele}[c]	19.96(3.63)	24.16(4.09)	9.01E-13
$-T\Delta S$	41.73(4.23)	39.48(3.98)	1.57E-04
$\Delta G_{binding}$[d]	−13.53(3.79)	−8.10(4.27)	9.10E-18

[a] Numbers in parentheses represent standard deviation

[b] Polar/nonpolar ($\Delta G_{sol} = \Delta G_{nonpolar} + \Delta G_{polar}$) contributions

[c] Total electrostatic energy ($\Delta G_{ele} = \Delta E_{ele} + \Delta G_{polar}$) contributions to the binding free energy

[d] Binding free energy ($\Delta G_{binding} = \Delta E_{vdW} + \Delta E_{ele} + \Delta G_{sol} - T\Delta S$)

[e] Statistical significance (*P*-value) was calculated by the *t*-test

($\Delta G_{nonpolar}$) of the solvation energy. However, of these three items of favorable energy contributions, the ΔE_{vdW} item contributes most to $\Delta G_{binding}$. This evidence is obviously reminiscent of the chemical composition of lapatinib, which consists mainly of four hydrophobic aromatic rings, including benzyl, aniline, quinazoline, and furan groups (Fig. 1b). Thus, the main interactions between lapatinib and HER2 were dominated by hydrophobic ΔE_{vdW} interactions. In addition, the total solvation energy ($\Delta G_{solvation}$) was unfavorable for the two systems. For example, the predicted values of $\Delta G_{solvation}$ are 40.37 ± 3.27 and 37.84 ± 3.83 kcal mol^{-1} for the WT HER2/lapatinib and L755P HER2/lapatinib complexes, respectively. In fact, the ligand and protein are wrapped by water molecules in solution and, prior to binding to the active site of a specific protein, the ordered structural water molecules around the surface of the ligand must be excluded. This process causes loss of $\Delta G_{binding}$. Because the total favorable energy contributions from molecular mechanics prevails over the unfavorable $\Delta G_{solvation}$, a bound protein–ligand complex would be formed. As can be seen from the Table 1, the predicted $\Delta G_{binding}$ values of lapatinib to WT and L755P mutant were -13.53 ± 3.79 and -8.10 ± 4.27 kcal mol^{-1}, respectively. The total $\Delta G_{binding}$ for the WT complex was 5.43 kcal mol^{-1} lower than that of the L755P complex. This result indicates that the L755P mutation generates a less energy-favorable complex that would result in weak binding of lapatinib to HER2 [42].

Table 2 Energy contributions to the binding energy (kcal mol^{-1}) of key individual residues[a]

Residue	WT	L755P	P-value[b]
Leu726	−2.53(0.50)	−1.49(0.41)	1.54E-37
Gly727	−1.39(0.38)	−0.22(0.24)	1.66E-65
Ser728	−1.52(0.42)	−0.14(0.09)	4.13E-80
Gly729	−1.21(0.28)	−0.09(0.02)	3.18E-96
Val734	−1.97(0.26)	−2.05(0.28)	0.039
Ala751	−1.11(0.33)	−1.21(0.25)	0.017
Lys753	−1.82(0.30)	−1.81(0.27)	0.81
Leu785	−1.71(0.25)	−1.73(0.29)	0.60
Leu796	−1.19(0.22)	−1.08(0.23)	7.12E-03
Thr798	−1.38(0.41)	−1.27(0.37)	0.049
Leu800	−2.14(0.32)	−2.23(0.26)	0.031
Met801	−2.20(0.34)	−2.22(0.36)	0.69
Cys805	−1.72(0.29)	−1.90(0.43)	6.78E-04
Leu852	−2.18(0.32)	−2.24(0.29)	0.17
Thr862	−1.01(0.22)	−0.74(0.30)	1.08E-11
Asp863	−1.03(0.18)	−0.62(0.26)	4.92E-28

[a] Numbers in the parentheses represent standard deviation

[b] Statistical significance (P-value) was calculated by t-test

Fig. 5 **a** Decomposition of $\Delta G_{binding}$ on an individual residue for the WT (black) and L755P (red) systems. **b** Detailed interactions between lapatinib and HER2 for the WT and L755P systems. Green dotted line Hydrogen bond between lapatinib and Met801
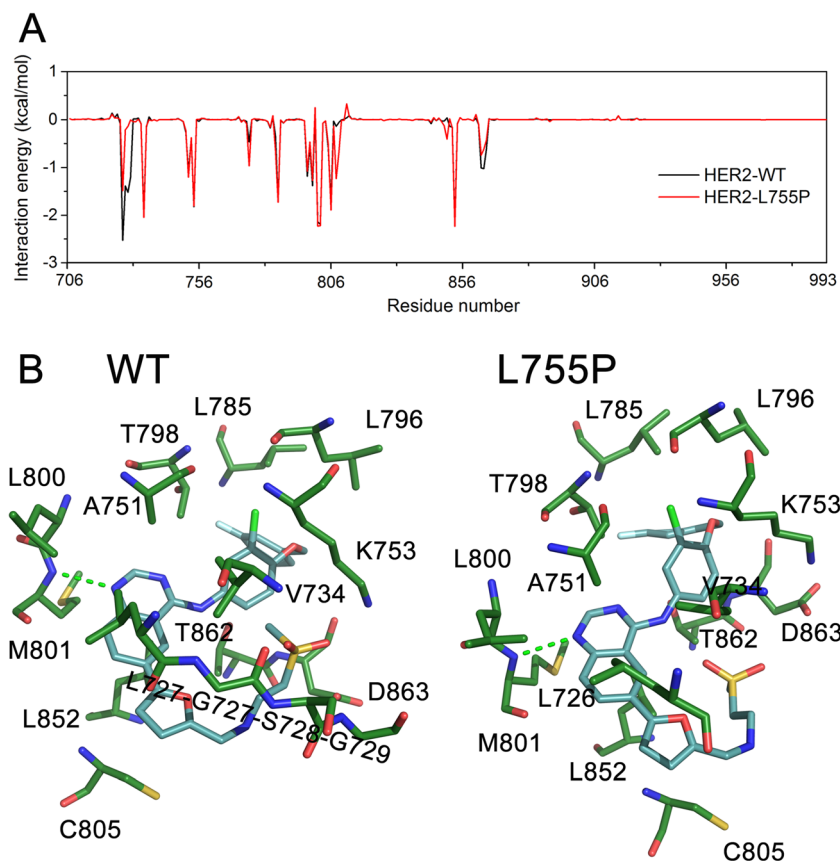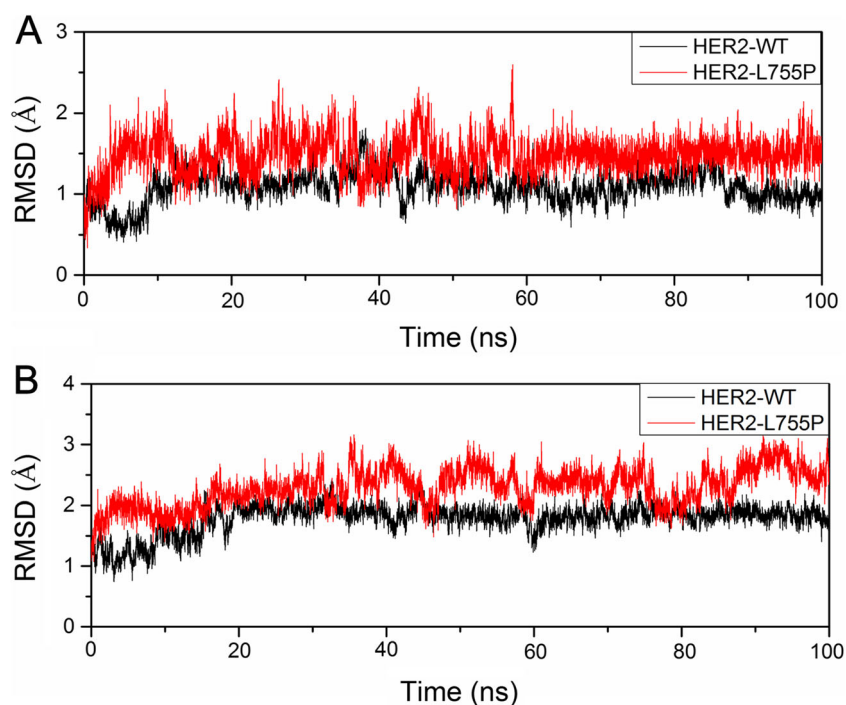
Fig. 6 Cα atoms RMSD of **a** helix αC and **b** the A loop for the WT (*black*) and L755P mutated (*red*) systems

Lapatinib-residue interaction decomposition

Understanding the individual residue decomposition of $\Delta G_{\text{binding}}$ will give us more detailed information pertaining to interactions between lapatinib and HER2. Figure 5a shows the interaction energy plot between lapatinib and HER2 for the two systems, and Table 2 lists the main residues that contributed to the binding. By comparing the per residue energy contribution to the $\Delta G_{\text{binding}}$ between the WT and L755P systems, it can be seen from Table 2 that the major differences come from residues Leu726, Gly727, Ser728, and Gly729, which belong to the G loop. As shown in Fig. 5b, residues Leu726, Gly727, Ser728, and Gly729 interact with the solubilizing group of lapatinib in the WT system. In contrast, in the L755P system, residues Gly727,

Ser728, and Gly729 form no contact with the solubilizing group of lapatinib. Despite the formation of the hydrophobic contact between residue Leu726 and the solubilizing group of lapatinib, the interaction energy in the mutated system is weaker than that of the WT system. Overall, the results of per residue decomposition are consistent with the structural analysis.

Discussion

Cancer is a global health problem and many people in both developed and developing countries suffer from this devastating disease. Currently, chemotherapy and targeted therapies have been developed to treat cancer patients [43]. However,

Fig. 7 Two-dimensional (2D) RMSD plots of the G loop, helix αC, and A loop for **a** WT and **b** L755P HER2
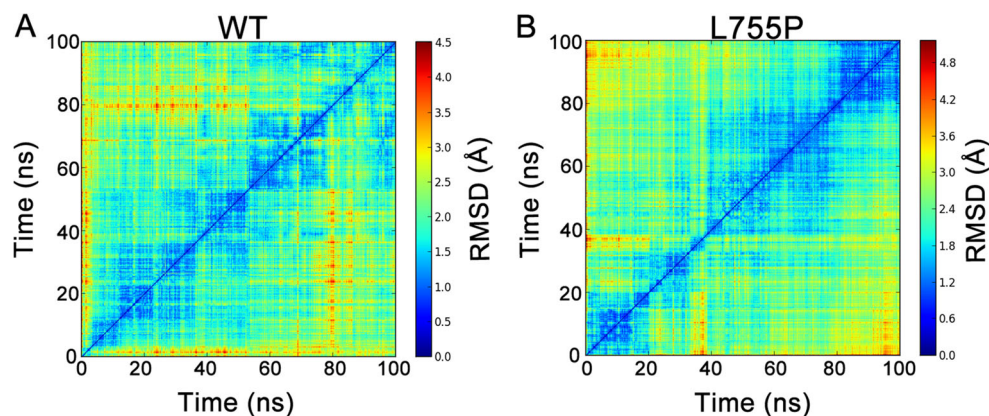
Fig. 8 Dynamic cross-correlation map (DCCM) for **a** WT and **b** L755P mutated systems. The regions of motion for the helix αC, G loop, and A loop in the L755P mutated system were increased significantly compared to those in the WT system. The value of correlation is in the range from −1 to 1. Positive values suggest positively correlated movement (same direction), while negative values suggests anti-correlated movement (opposite direction)
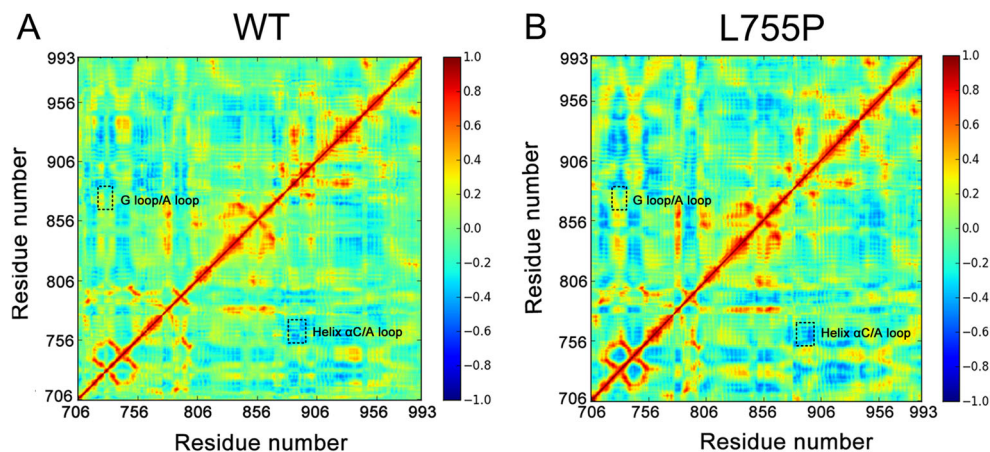
the emergence of resistance to chemotherapy and molecularly targeted therapies remains a major concern in the treatment of cancer; therein, mutations in the drug target have been observed frequently in the field of drug-resistance to cancer therapies. For example, 1,356 unique mutations involved in drug-resistance in 116 drug targets have been reported in the Cancer Drug Resistance Database (CancerDR) [44]. Thus, insight into the mechanisms of drug-resistance observed in specific drug targets is nowadays an urgent and active topic in the development of effective cancer therapies.

Over-expression of PTKs has been closely implicated in cancers, rendering PTKs effective therapeutic drug targets for the treatment of cancer [1, 6]. For example, the HER2 receptor tyrosine kinase—a member of the ErbB protein family—plays a critical role in the pathogenesis of many human cancers [15, 16]. However, the HER2 L755P mutation causes drug-resistance to the ATP-competitive inhibitor lapatinib. The mechanisms of drug-resistance remain currently unresolved, but mutations in these proteins could lead to structural changes that may explain the emergence of drug-resistance. Therefore, unraveling how the L755P mutation causes structural changes in the HER2 may provide an opportunity to solve some drug-resistance problems in cancers. As such, MD simulations have proved successful in capturing the conformational changes of macromolecules as well as unveiling the structure and function of proteins [45–49]. Consequently, we harnessed MD simulations to illuminate the impact of the L755P mutation on the structural dynamics of HER2.

Through RMSD analysis, we found that the L755P mutation indeed caused structural changes in HER2 relative to WT HER2. Further RMSF analysis revealed that the main structural fluctuations occurred in the regions of the helix αC, the G loop, and the A loop. Superimposition of the representative structures between the HER2 WT and L755P mutated complexes also demonstrated the structural changes in these regions. Furthermore, as shown in Fig. 6, the values of Cα atoms RMSD for helix αC and the A loop in the L755P mutated system were larger compared to those in the WT

system. Moreover, analysis of two-dimensional (2D) RMSD plots for the two simulated systems showed the all-against-all RMSD values between each of the conformations at a specific frame number. Each color point represents the RMSD between the frame conformation on the x-axis and the frame conformation on the y-axis [50]. As shown in Fig. 7, the 2D RMSD plots of Cα atoms of the G loop, helix αC, and A loop indicated the existence of conformational arrangements in the L755P mutated HER2 as compared to WT HER2. In addition, the dynamic features of the WT and L755P mutated HER2 in the simulations generate information about correlated motion that is useful for analysis [36]. Correlated motions can occur among proximal residues and also between regions, e.g., in domain–domain communications. To reveal the range of correlated motions, we plotted a dynamic cross-correlation map (DCCM) for the Cα atoms of residues for the two simulated systems (Fig. 8). As shown in Fig. 8a, in WT HER2, the G loop and A loop regions have positive correlations (moving in the same direction), while correlations of the helix αC and A loop regions were negative (moving in the opposite direction). However, in L755P HER2 (Fig. 8b), the G loop and A loop regions as well as helix αC and the A loop exhibited increases
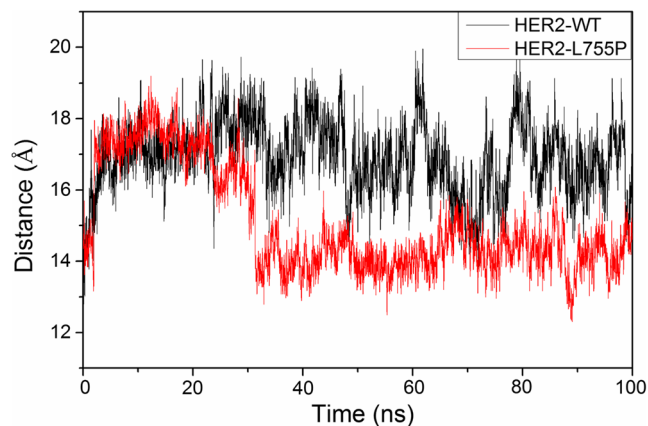

Fig. 9 Time dependence of the distance between the Cα atoms of Glu757 and Gly865 in WT and L755P HER2

in both positive and negative correlations, respectively, compared to WT HER2. These data suggested the existence of strong structural coupling of the G loop, helix αC, and A loop in HER2 due to the L755P mutation. As shown in Fig. 3, movement of the helix αC towards the G loop caused the collapse of the G loop into the ATP-binding site in the HER2 L755P system, which in turn led to the orientation of the solubilizing group of lapatinib into the interior of the ATP-binding site (Fig. 5b). To further elucidate the arrangement of the helix αC in L755P HER2, the Cα atom distance of residues Glu757 and Gly864 (DFG motif) were monitored. As shown in Fig. 9, in WT HER2, the distance between Glu757 and Gly864 fluctuates at ~16.9±1.0 Å along the 100 ns MD simulations. In L755P HER2, in the first 30 ns simulation, the distance is 17.0±0.9 Å. However, the distance reduces to 15.5±0.6 Å in the period of 30 ns to 100 ns. This is due to the fact that the helix αC has moved towards the C lobe in response to the L755P mutation (Fig. 3). In addition, MM-GBSA binding free energy calculations revealed that the L755P mutation caused a significant loss of binding ability of lapatinib to HER2 compared to the WT system. Moreover, the major differences in the contribution of specific residues to binding came from residues in the G loop. Together, these data indicate that the HER2 L755P mutation leads to drug-resistance to lapatinib.

Conclusions

In the present study, molecular docking, MD simulations, and MM-GBSA binding free energy calculations were performed to investigate the mechanism of drug-resistance to lapatinib due to the HER2 L755P mutation. MD simulations showed that the L755P mutation caused structural changes in the helix αC, G loop, and A loop regions. Especially, movement of the helix αC towards the G loop led to the collapse of the G loop into the ATP-binding site, thereby disrupting the interactions between the solubilizing group of lapatinib and residues in the G loop in the L755P mutated system. MM-GBSA binding free energy calculations revealed that the main interactions between lapatinib and HER2 were derived mainly from hydrophobic interactions. The L755P mutation resulted in the loss of approximately 5 kcal mol^{-1} binding free energy compared to the WT system, which may cause the weak binding of lapatinib to the mutated HER2. Moreover, the loss of energy contributions in the L755P mutated system stemmed primarily from residues in the G loop, in agreement with the structural analysis. The results obtained provide helpful insights into the mechanism of drug-resistance in HER2 and will inform the design of the next-generation of HER2 inhibitors.

References

1. Schlessinger J, Lemmon MA (2006) Nuclear signaling by receptor tyrosine kinases: the first robin of spring. Cell 127:45–48
2. Roskoski R Jr (2014) The ErbB/HER family of protein-tyrosine kinases and cancer. Pharmacol Res 79:34–74
3. Tao R-H, Maruyama IN (2008) All EGF(ErbB) receptors have performed homo- and heterodimeric structures in living cells. J Cell Sci 121:3207–3217
4. Dawson JP, Berger MB, Lin CC, Schlessinger J, Lemmon MA, Ferguson KM (2005) Epidermal growth factor receptor dimerization and activation require ligand-induced conformational changes in the dimer interface. Mol Cell Biol 25: 7734–7742
5. Seshacharyulu P, Ponnusamy MP, Haridas D, Jain M, Ganti AK, Batra SK (2012) Targeting the EGFR signaling pathway in cancer therapy. Expert Opin Ther Targets 16:15–31
6. Baselga J (2006) Targeting tyrosine kinases in cancer: the second wave. Science 312:1175–1178
7. Oqiso H, Ishitani R, Nureki O, Fukai S, Yamanaka M, Kim JH, Saito K, Sakamoto A, Inoue M, Shirouzu M, Yokoyama S (2002) Crystal structure of the complex of human epidermal growth factor and receptor extracellular domains. Cell 110: 775–787
8. Oxnard GR, Miller VA (2010) Use of erlotinib or gefitinib as initial therapy in advanced NSCLC. Oncology 24:392–399
9. Wainberg ZA, Anghel A, Desai AJ, Ayala R, Luo T, Safran B, Fejzo MS, Hecht R, Slamon DJ, Finn RS (2010) Lapatinib, a dual EGFR and HER2 kinase inhibitor, selectively inhibits HER2-amplified human gastric cancer cell and is synergistic with trastuzumab in vitro and in vivo. Clin Cancer Res 16: 1509–1519
10. Gorre ME, Mohammed M, Ellwood K, Hsu N, Paquette R, Rao PN, Sawyers CL (2001) Clinical resistance to STI-571 cancer therapy caused by BCR-ABL gene mutation or amplification. Science 293: 876–880
11. Ma C, Wei S, Song Y (2011) T790M and acquired resistance of EGFR TKI: a literature review of clinical reports. J Thorac Dis 3: 10–18
12. Avizienyte E, Ward RA, Garner AP (2008) Comparison of the EGFR resistance mutation profiles generated by EGFR-targeted tyrosine kinase inhibitors and the impact of drug combinations. Biochem J 145:197–206
13. Yun CH, Mengwasser KE, Toms AV, Woo MS, Greulich H, Wong KK, Meyerson M, Eck MJ (2008) The T790M mutation in EGFR kinase domain causes drug resistance by increasing the affinity for ATP. Proc Natl Acad Sci USA 105: 2070–2075
14. Bean J, Riely GJ, Balak M, Marks JL, Ladanyi M, Miller VA, Pao W (2008) Acquired resistance to epidermal growth factor receptor kinase inhibitors associated with a novel T854A mutation in a patient with EGFR-mutant lung adenocarcinoma. Clin Cancer Res 14: 7519–7525
15. Gilmer TM, Cable L, Alligood K, Rusnak D, Spehar G, Gallagher KT, Woldu E, Carter HL, Truesdale AT, Shewchuk L, Wood ER (2008) Impact of common epidermal growth factor receptor and HER2 variants on receptor activity and inhibition by lapatinib. Cancer Res 68:571–579
16. Trowe T, Boukouvala S, Calkins K, Cutler RE, Ryan Fong C Jr, Funke R, Gendreau SB, Kin YD, Miller N, Woodlfrey JR, Vysotskaia V, Yang JP, Gerritsen ME, Matthews DJ, Lamb P, Heuer TS (2008) EXEL-7647 inhibits mutant forms of ErbB2 associated with lapatinib resistance and neoplastic transformation. Clin Cancer Res 14:2465–2475

17. Stephens P, Hunter C, Biqnell G, Edkins S, Davies H, Teaque J, Stevens C, O'Meara S, Smith R, Parker A, Barthorpe A, Blow M, Brackenbury L, Butler A, Clarke O, Cole J, Dicks E, Dike A, Drozd A, Edwards K, Forbes S, Foster R, Gray K, Greenman C, Halliday K, Hills K, Kosmidou V, Lugg R, Menzies A, Perry J, Petty R, Raine K, Ratford L, Shepherd R, Small A, Stenphens Y, Tofts C, Varian J, West S, Widaa S, Yates A, Brasseur F, Cooper CS, Flanagan AM, Knowles M, Leung SY, Louis DN, Looijenga LH, Malkowicz B, Pierotti MA, Teh B, Chenevix-Trench G, Weber BL, Yuen ST, Harris G, Goldstraw P, Nicholson AG, Futreal PA, Woodster R, Stratton MR (2004) Lung cancer: intragenic ERBB2 kinase mutations in tumours. Nature 431:525–526

18. Aertgeerts K, Skene R, Yano J, Sang B-C, Zou H, Snell G, Jennings A, Iwamoto K, Habuka N, Hirokawa A, Ishikawa T, Tanaka T, Miki H, Ohta Y, Sogabe S (2011) Structural analysis of the mechanism of inhibition and allosteric activation of the kinase domain of HER2 protein. J Biol Chem 186:18756–18765

19. Fiser A, Do RK, Sali A (2000) Modeling loops in protein structures. Protein Sci 9:1753–1773

20. Frisch MJ, Trucks GW, Schlegel HB, Scuseria GE, Robb MA, Cheeseman JR, Montgomery JA Jr, Vreven T, Kudin KN, Burant JC, Millam JM, Iyengar SS, Tomasi J, Barone V, Mennucci B, Cossi M, Scalmani G, Rega N, Petersson GA, Nakatsuji H, Hada M, Ehara M, Toyota K, Fukuda R, Hasegawa J, Ishida M, Nakajima T, Honda Y, Kitao O, Nakai H, Klene M, Li X, Knox JE, Hratchian HP, Cross JB, Adamo C, Jaramillo J, Gomperts R, Stratmann RE, Yazyev O, Austin AJ, Cammi R, Pomelli C, Ochterski JW, Ayala PY, Morokuma K, Voth GA, Salvador P, Dannenberg JJ, Zakrzewski VG, Dapprich S, Daniels AD, Strain MC, Farkas O, Malick DK, Rabuck AD, Raghavachari K, Foresman JB, Ortiz JV, Cui Q, Baboul AG, Clifford S, Cioslowski J, Stefanov BB, Liu G, Liashenko A, Piskorz P, Komaromi I, Martin RL, Fox DJ, Keith T, Al-Laham MA, Peng CY, Nanayakkara A, Challacombe M, Gill PMW, Johnson B, Chen W, Wong MW, Gonzalez C, Pople JA (2003) Guassian 03. Gaussian, Inc., Wallingford

21. Morris GM, Huey R, Lindstrom W, Sanner MF, Belew RK, Goodsell DS, Olson AJ (2009) AutoDock4 and AutoDockTools4: automated docking with selective receptor flexibility. J Comput Chem 30:2785–2791

22. Lu S, Huang W, Li X, Huang Z, Liu X, Chen Y, Shi T, Zhang J (2012) Insights into the role of magnesium traid in myo-inositol monophosphatase: metal mechanism, substrate binding, and lithium therapy. J Chem Inf Model 52: 2398–2409

23. Lu S, Huang W, Wang Q, Shen Q, Li S, Nussinov R, Zhang J (2014) The structural basis of ATP as an allosteric modulator. PLoS Comput Biol 10:e1003831

24. Case DA, Darden TA, Cheatham TE III, Simmerling CL, Wang J, Duke RE, Luo R, Walker RC, Zhang W, Merz KM, Roberts BP, Wang B, Hayik S, Roitberg A, Seabra G, Kolossvary I, Wong KF, Paesani F, Vanicek J, Liu J, Wu X, Brozell SR, Steinbrecher T, Gohlke H, Cai Q, Ye X, Wang J, Hsieh MJ, Cui G, Roe DR, Mathews DH, Seetin MG, Sagui C, Babin V, Luchko T, Gusarov S, Kovalenko A, Kollman PA (2010) AMBER 11. University of California, San Francisco

25. Duan Y, Wu C, Chowdhury S, Lee MC, Xiong G, Zhang W, Yang R, Cieplak P, Luo R, Lee T (2003) A point-charge force field for molecular mechanics simulations of proteins. J Comput Chem 24:1999–2012

26. Wang J, Wolf RM, Caldwell JW, Kollman PA, Case DA (2004) Development and testing of a general amber force field. J Comput Chem 25:1157–1174

27. Jorgensen WL, Chandrasekhar J, Madura JD, Impey RW, Klein ML (1983) Comparison of single potential function for simulating liquid water. J Chem Phys 79:926–935

28. Darden T, York D, Pedersen L (1993) Particle mesh Ewald: an N log(N) method for Ewald sums in large systems. J Chem Phys 98: 10089–10092

29. Ryckaert JP, Ciccotti G, Berendsen HJC (1977) Numerical integration of the cartesian equations of motion of a system with constraints: molecular dynamics of n-alkanes. J Comput Phys 23:327–341

30. Wu X, Brooks BR (2003) Self-guided Langevin dynamics simulation method. Chem Phys Lett 381:512–518

31. Huang Y, Rizzo RC (2012) A water-based mechanism of specificity and resistance for lapatinib with ErbB family kinases. Biochemistry 51:2390–2406

32. Ahmed M, Sadek MM, Abouzid KA, Wang F (2013) In silico design: extended molecular dynamic simulations of a new series of dually acting inhibitors against EGFR and HER2. J Mol Graph Model 44: 220–231

33. Sun H, Li Y, Tian S, Xu L, Hou T (2014) Assessing the performance of MM/PBSA and MM/GBSA methods. 4. Accuracies of MM/PBSA and MM/GBSA methodologies evaluated by various simulation protocols using PDBbind data set. Phys Chem Chem Phys 16: 16719–16729

34. Bai Q, Pérez-Sánchez H, Zhang Y, Shao Y, Shi D, Liu H, Yao Y (2014) Ligand induced change of β2 adrenergic receptor from active to inactive conformation and its implication for the closed/open state of the water channel: insight from molecular dynamics simulation, free energy calculation and Markov state model analysis. Phys Chem Chem Phys 16:15874–15885

35. Shao J, Tanner SW, Thompson N, Cheatham TEIII (2007) Clustering molecular dynamics trajectories: 1. Characterizing the performance of different clustering algorithms. J Chem Theory Comput 3: 2312–2334

36. Luo J, Bruice T (2002) Ten-nanosecond molecular dynamics simulation of the motions of the horse liver alcohol dehydrogenase•PhCH2O- complex. Proc Natl Acad Sci USA 99: 16597–16600

37. Li X, Wang X, Tian Z, Zhao H, Liang D, Li W, Qiu Y, Lu S (2014) Structural basis of valmerins as dual inhibitors of GSK3β/CDK5. J Mol Model 20:2407

38. Palmieri L, Rastelli G (2013) αC helix displacement as a general approach for allosteric modulator of protein kinases. Drug Discov Today 18:407–414

39. Lu S, Li S, Zhang J (2014) Harnessing allostery: a novel approach to drug discovery. Med Res Rev 34:1242–1285

40. Adams JA (2003) Activation loop phosphorylation and catalysis in protein kinases: is there functional evidence for the autoinhibitor model? Biochemistry 42:601–607

41. Nolen B, Taylor S, Ghosh G (2004) Regulation of protein kinases. Mol Cell 15:661–675

42. Lu S, Jiang Y, Lv J, Zou J, Wu T (2011) Mechanism of kinase inactivation and nonbinding of FRATide to GSK3β due to K85M mutation: molecular dynamics simulation and normal mode analysis. Biopolymers 95:669–681

43. Yap TA, Carden CP, Kaye SB (2009) Beyond chemotherapy: targeted therapies in ovarian cancer. Nat Rev Cancer 9:167–181

44. Kumar R, Chaudhary K, Gupta S, Singh H, Kumar S, Gautam A, Kapoor P, Raghava GPS (2014) CancerDR: cancer drug resistance database. Sci Rep 3:1445

45. Sun H, Li Y, Tian S, Wang J, Hou T (2014) P-loop conformation governed crizotinib resistance in G2032R-mutated ROS1 tyrosine kinase: clues from free energy landscape. PLoS Comput Biol 10: e1003729

46. Shao S, Yu R, Yu Y, Li Y (2014) Dual-inhibitors of STAT5 and STAT3: studies from molecular docking and molecular dynamics simulations. J Mol Model 20:2399

47. Lu S, Huang W, Zhang J (2014) Recent computational advances in the identification of allosteric sites in proteins. Drug Discov Today 19:1595–1600

48. Li J, Rossetti G, Dreyer J, Raugei S, Ippolitti E, Lüscher B, Carloni P (2014) Molecular simulation-based structural prediction of protein complexes in mass spectrometry: the human insulin dimer. PLoS Comput Biol 10:e1003838

49. Chebaro Y, Amal I, Rochel N, Rochette-Egly C, Stote RH, Dejaegere A (2013) Phosphorylation of the retinoic acid receptor alpha induces a mechanical allosteric regulation and changes in internal dynamics. PLoS Comput Biol 9:e1003012

50. Koch O, Cappel D, Nocker M, Jäger T, Flohé L, Sotriffer CA, Selzer PM (2013) Molecular dynamics reveal binding mode of glutathionylspermidine by trypanothione synthetase. PLoS One 8: e56788

51. Onufriev A, Bashford D, Case DA (2004) Exploring protein native states and large-scale conformational changes with a modified generalized Born model. Proteins 55: 383–394